THE JOURNAL OF PHYSICAL CHEMISTRY Letters

Letter

pubs.acs.org/JPCL

Capturing the Ultrafast Vibrational Decoherence of Hydrogen Bonding in Interfacial Water

Abdelaziz Boulesbaa and Eric Borguet*

Department of Chemistry, Temple University, 1901 North 13th Street, Philadelphia, Pennsylvania 19122, United States

Supporting Information

ABSTRACT: Vibrational sum-frequency generation (vSFG) measurements in the frequency and time domains reveal that the interfacial hydrogen bonded OH stretch at the water/calcium fluoride interface is composed of two populations oriented oppositely. The time-resolved vSFG free-induction decay suggested that, whereas the strongly hydrogen bonded OH vibrational stretches, centered near 3140 ± 11 cm^{-1}, are oriented toward bulk water and lose their collective coherence within ~70 ± 7 fs, the weakly hydrogen bonded OH species, centered near 3410 ± 12 cm^{-1}, are pointed toward the interface and dephase within ~50 ± 6 fs.

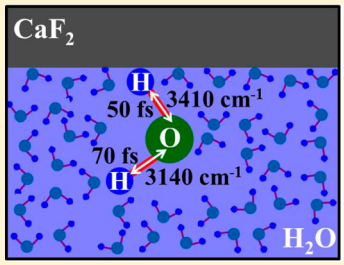

Water is the liquid most investigated by the scientific community, not only because it is indispensable for life, but due to its wide and diverse applications.[1−3] In many circumstances, water is interfaced with different materials. In chemistry, water is widely used as a solvent.[4] In biology, it hydrates cells and biomolecules.[1] In solar cells, it is interfaced with metals and semiconductors to produce hydrogen gas.[3,5] Many of the interesting properties arise from the hydrogen bonding (O−H) network.[6] Thus, understanding the flow and redistribution of vibrational energy through this network is crucial for the control of O−H bond formation and breaking.[7,8] A physical quantity that is sensitive to this spread of energy within the O−H network is the total dephasing time, T_2, which is directly related to the inhomogeneous line shape of the vibrational transition.[9,10] Since in the liquid phase water molecules are surrounded by other molecules that exert forces on them, they undergo ultrafast structural fluctuations that randomize the energy over the entire transition spectral line, an inhomogeneous broadening of the spectral line shape hides the dynamic information contained in the inhomogeneous line.[9,10] The pure dephasing time, T^*_2 (exclusively due to homogeneous broadening), of the O−H stretch vibration in liquid water was measured using the photon-echo technique to be on the order of 90 fs.[9,11] This sub-100 fs time-scale for OH dephasing in liquid water was confirmed by several calculations.[12−15]

For the case of interfacial water, because the inversion symmetry is broken at the surface, the approach used to investigate structural and dynamical behavior of vibrational O−H stretches is a surface specific nonlinear technique such as sum-frequency generation (SFG).[16−18] In frequency-domain SFG experiments, a mid-infrared ($\omega_{\text{mid-IR}}$) spectrally broad pulse resonantly promotes O−H stretches into the excited state, then a spectrally narrow pulse, in general in the visible (ω_{Vis}), upconverts the excited oscillators into an induced macroscopic polarization that can radiate at the sum-frequency $\omega_{\text{SFG}} = \omega_{\text{mid-IR}}+\omega_{\text{Vis}}$.[18] In order to measure the total vibrational dephasing T_2, given that $1/T_2 = 1/2T_1 + 1/T_2^*$, where T_1 is the vibrational lifetime, via the SFG technique,[19] the ultrashort mid-infrared pulse resonantly and coherently drives vibrational oscillators into the excited state, then another nonresonant ultrashort pulse upconverts the superposition of the ground and excited states into an SFG signal. The decay of SFG intensity versus $\Delta\tau$, the time-delay between the resonant mid-IR and the nonresonant upconverting pulses, is called a free induction decay (FID).[20]

Although several research efforts have targeted the investigation of ultrafast vibrational dynamics of interfacial water,[21−25] most reports concerned the measurements of population lifetime, T_1. In this Letter, we report on the measurement of the total vibrational dephasing time, T_2, of O−H stretches at the water/calcium fluoride (H_2O/CaF_2) interface using the FID-SFG technique with an unprecedented temporal resolution of ~20 fs. The neutral H_2O/CaF_2 interface was chosen to minimize the effect of ions[26] and to limit the SFG response to the O−H bonds of interfacial water molecules. Time-domain FID-SFG measurements suggested the presence of two populations of hydrogen bonded O−H vibrational modes. One low frequency species, attributed to strong hydrogen bonds oriented toward bulk water around ~3140 ± 11 cm^{-1}, dephases within ~70 ± 7 fs, and a second high frequency species around 3410 ± 12 cm^{-1} that dephases on a time-scale of ~50 ± 6 fs attributed to weakly hydrogen bonded water molecules pointing toward the CaF_2.

Prior to investigating the vibrational coherence of the hydrogen bonded OH stretch modes of interfacial water, we first carried out frequency-domain SFG measurements at the CaF_2/H_2O interface to reveal the vibrational modes present at this interface. The ultrabroadband mid-IR pulse shown in Figure 1A, which covers the frequency range 2900−4000 cm^{-1} with a fwhm ~640 cm^{-1}, is upconverted into Vis-SFG using the

Received: August 19, 2016
Accepted: November 23, 2016

DOI: 10.1021/acs.jpclett.6b01870
J. Phys. Chem. Lett. 2016, 7, 5080−5085

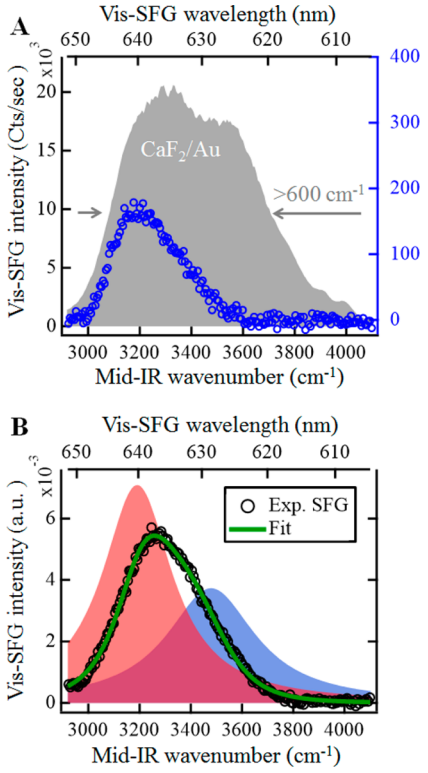

Figure 1. (A) Mid-IR spectrum obtained via Vis-SFG upconversion at the CaF_2/Au interface (shaded area), and Vis-SFG spectrum obtained at the CaF_2/H_2O interface (blue symbols). (B) Normalized Vis-SFG spectrum obtained at the CaF_2/H_2O interface (symbols) fit to eq 1 (solid line). Shaded areas are the two components of the fit. Each component is obtained making the amplitude of the other peak zero while fixing all the other parameters as obtained by the converged fit.

spectrally narrow visible pulse centered at ~804 nm. Based on its bandwidth of ~600 cm^{-1}, it is compressible to a transform limit of ~25 fs considering a Gaussian shaped pulse. In order to account for the mid-IR spectral profile, the Vis-SFG spectrum obtained from the CaF_2/H_2O sample is divided by that obtained from the reference sample (CaF_2/Au). The resulting normalized Vis-SFG spectrum is shown in Figure 1B. To reveal the vibrational oscillators contributing to this signal, the normalized Vis-SFG spectrum is fit to the following equation

$$I_{\text{Vis-SFG}} \propto \left| \sum_n \frac{A_n}{\omega_{\text{mid-IR}} - \omega_n + i(\Gamma_n + \Delta\omega_{\text{Vis}}/2)} + |A_{\text{NR}}|e^{i\phi} \right|^2 \quad (1)$$

where A_{NR}, φ, A_n, and Γ_n are the vibrationally nonresonant susceptibility amplitude, the phase between the resonant and nonresonant contributions, and the amplitude and damping constant of the surface vibration with frequency ω_n, respectively; $\omega_{\text{mid-IR}}$ and $\Delta\omega_{\text{Vis}}$ are the driving mid-IR pulse frequency components and the bandwidth of the upconverting visible pulse, centered at 804 nm, respectively.[20]

The converged fit returned the parameters listed in Table 1, which suggests the presence of two vibrational modes; one centered around 3190 cm^{-1} with negative amplitude, and the other centered around 3480 cm^{-1}, with positive amplitude. Based on the reported assignments of SFG peak components at the air/H_2O and CaF_2/H_2O interfaces,[27] the high frequency peak is

Table 1. Amplitude A_n, Frequency ω_n, and Lorentzian Half-Width at Half Maximum (HWHM) Γ_n of the nth Mode from Fit by Eq 1 of the Vis-SFG Spectrum of CaF_2/H_2O Shown in Figure 1B[a]

A_n	ω_n (cm^{-1})	Γ_n (cm^{-1})	$T_{2,n}$ (fs)
−14.0 ± 1.4	3190.5 ± 0.6	158.6 ± 19.3	33.5 ± 5.4
+12.9 ± 0.7	3479.0 ± 19.5	203.1 ± 3.3	26.1 ± 0.5

[a]The values of A_{NR} and ϕ were 0.3×10^{-3} and π, respectively. $T_{2,n}$ is the total dephasing time estimated based on $T_{2,n} = 1/2\pi c\Gamma_n$.[29] The uncertainty values are based on the standard deviation determined from two independent experiments.

attributed to weakly hydrogen bonded OH stretch modes pointing toward the interface, whereas the low frequency peak describes the strongly hydrogen bonded OH vibrational stretch transition dipole pointing toward surrounding bulk water molecules.[27] Based on the half-width at half-maximum (HWHM), Γ_n, of each peak, the estimated total dephasing time, T_2, of strongly hydrogen bonding OH stretch is on the order of ~34 fs, and the dephasing time of weakly hydrogen bonding OH stretch is on the order of ~26 fs.[28]

Although conventional frequency-domain SFG measurements can predict the total dephasing time, $T_{2,n}$, based on the spectral width of the vibrational transitions via Fourier transform when sufficient spectral resolution is available to accurately determine lineshapes,[30,31] time-domain FID-SFG measurements when they are carried out with sufficient signal-to-noise ratio, delay range, and more importantly temporal resolution, are preferred due to their capability not only to extract, $T_{2,n}$, but also potentially the relative orientations of the vibrational oscillators that contribute to the macroscopic polarization. Noting that although phase-sensitive frequency-domain SFG is capable of extracting the orientation information as well, FID-SFG is simpler to implement when sufficient temporal resolution is available.[22,26]

Based on the estimated values of $T_{2,n}$ (total dephasing times) listed in Table 1, a temporal resolution at least on the order of ~30 fs is indispensable in measuring FID-SFG dynamics. To achieve that, the spectrally broad mid-IR and NIR outputs of NOPA1 and NOPA2, respectively, were compressed in the time-domain nearly to their transform limit.[20,32] Shown in Figure 2A are the NIR-SFG spectra obtained as SFG cross correlations between the mid-IR and NIR pulses at the CaF_2/Au interface at a few discrete time-delays. To obtain the instrument response function (IRF), the average intensity of each NIR-SFG spectrum at each time-delay is plotted in Figure 2B. The full-width at half-maximum (fwhm) of the IRF plot is ~32 ± 4 fs, suggesting that the pulse duration is on the order of 22 fs.[32] This temporal resolution is sufficient to resolve the expected total dephasing times $T_{2,n}$, projected to be on the ~34 and ~26 fs time-scales for strongly and weakly hydrogen bonded O−H stretches, respectively.

After achieving a temporal resolution sufficient for resolving the expected sub-50 fs dephasing dynamics of interfacial water OH vibrational stretches, FID-SFG measurements at the CaF_2/H_2O interface were carried out, and the results are shown in Figure 3B. At negative time-delays, the growth of the FID-SFG signal is slower than that of the IRF. In fact, the FID-SFG signal did not reach its maximum amplitude until about ~40 fs later. This effect can be explained by the presence of two vibrational modes with opposite phases, which suggests the presence of two distinct types of OH oscillators oriented oppositely, and because they have comparable strength they cancel each other, leading to

DOI: 10.1021/acs.jpclett.6b01870
J. Phys. Chem. Lett. 2016, 7, 5080−5085

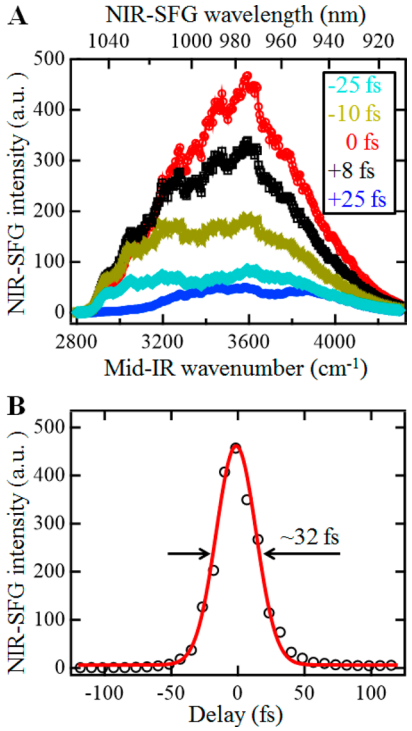

Figure 2. (A) NIR-SFG spectra at different time-delays between the mid-IR and NIR pulses as indicated. (B) The intensity average of NIR-SFG spectra versus time-delays describing the instrument response function at the CaF_2/Au interface (symbols). The solid line is a Gaussian fit with a full width at half-maximum of ~32 ± 4 fs, corresponding to a pulse duration of ~22 ± 3 fs.

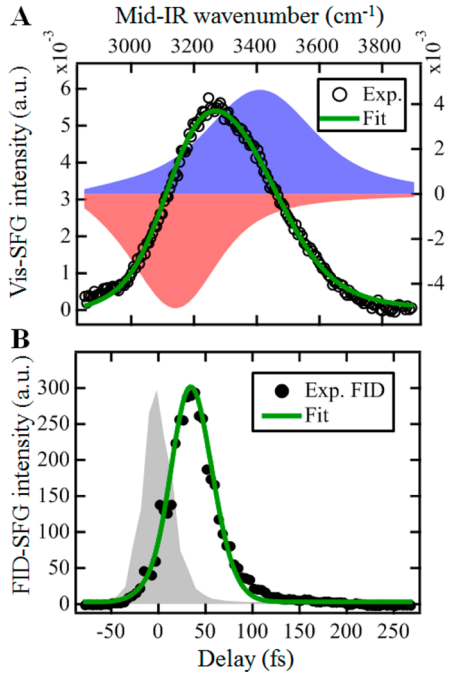

Figure 3. (A) Normalized Vis-SFG spectrum of the OH vibrational stretch at the CaF_2/H_2O interface (symbols) with the intensity axis on the left side. The two shaded areas indicate the two spectral components of the fit with the intensity axis on the right side. Each component is obtained making the amplitude of the other peak zero while fixing all the other parameters as obtained by the converged fit. (B) FID-SFG dynamics at the CaF_2/H_2O interface (symbols). The shaded area is the instrument response function. The solid lines in A and B are the result of a simultaneous fit to spectral and time domain data.

a negligible signal at time zero that increases as the oscillators move out of phase opposition due to their distinct natural frequencies.[20,33] It is important to note that the information extracted here concerns the relative but not the absolute phases. Thereafter, the FID-SFG signal decays nonexponentially after reaching its maximum amplitude, which can be a manifestation of inhomogeneous contribution to the broadening of the line-width.[20,30,34]

To account for an additional contribution to the broadening of the vibrational line width, an inhomogeneous term ($\Gamma_{inh,n}$) was added to the homogeneous line-width (Γ_n) for each vibrational mode in eq 1. To correlate time and frequency domain SFG measurements, a simultaneous fit of the normalized frequency-domain Vis-SFG spectrum (shown in Figure 1B) and time-domain FID-SFG dynamics[20,29,34] was performed, the results of which are shown in Figure 3A,B. In carrying out this fit, the function describing the Vis-SFG spectrum is expressed in eq 2 and contains a convolution (conv) of a Gaussian and a Lorentzian to account for the inhomogeneous broadening

$$I_{SFG} \propto \left| \sum_n \mathrm{conv}\left(\frac{A_n}{\omega_{\text{mid-IR}} - \omega_n + i(\Gamma_n + \Delta\omega_{Vis}/2)} \times \exp\left\{ -\left(\frac{\omega_{\text{mid-IR}} - \omega_n}{\Gamma_{inh,n}} \right)^2 \right\} \right) + \frac{|A_{NR}|}{\Delta\omega_{\text{mid-IR}}} e^{i\phi} \right|^2 \quad (2)$$

where $\Delta\omega_{\text{mid-IR}}$ is the width of the mid-IR pulse. For fitting the FID-SFG dynamics, the following equation is used:[20,30,34]

$$I_{\text{FID-SFG}}(\Delta\tau) \propto \int_{-\infty}^{\infty} dt |P^{(2)}(t, \Delta\tau)|^2 \quad (3a)$$

$$P^{(2)}(t, \Delta\tau) \propto E_{NIR}(t - \Delta\tau) P^{(1)}(t) \quad (3b)$$

$$P^{(1)}(t) = \int_{-\infty}^{\infty} dt' E_{\text{mid-IR}}(t - t') R(t') \quad (3c)$$

where the second-order polarization, $P^{(2)}$, at a given time-delay, $\Delta\tau$, expressed in eq 3b is created by mixing the first-order polarization $P^{(1)}$ induced by the mid-IR ($E_{\text{mid-IR}}$) excitation and the polarization induced by the NIR upconverting field (E_{NIR}) as expressed in eq 3c.[20,30,34]

$$R(t) = \{\delta(t)|A_{NR}| \exp(i\phi) - i\theta(t) \sum_n A_{R,n} \exp[2\pi c(-i\omega_n t - \Gamma_n t)] \times \exp[-(2\pi c \Gamma_{inh,n} t)^2]\} + \text{c.c.} \quad (3d)$$

During the simultaneous fit, the center frequency of each vibrational mode, the phase, homogeneous line width, and inhomogeneous line width in eqs 2 and 3a are linked to each other, and $\Delta\omega_{\text{mid-IR}}$ and $\Delta\omega_{Vis}$ are fixed at 600 and 16 cm^{-1}, respectively, based on their experimentally determined values.

We considered the hypothesis that the spectrum describes one chemical species and attempted to perform the simultaneous fit using one vibrational oscillator. Although the resulting converged fit, shown in Figure S1 in the Supporting Information, acceptably describes the frequency-domain Vis-SFG spectrum, it did not well fit the time-domain FID-SFG dynamics. Mainly, at negative time-delays, the rise of the simulated signal was similar to the IRF

DOI: 10.1021/acs.jpclett.6b01870
J. Phys. Chem. Lett. 2016, 7, 5080−5085

Table 2. Amplitude A_n, Frequency ω_n, Lorentzian Half-Width at Half Maximum (HWHM) Γ_n, Dephasing Time $T^*_{2,n}$, and Inhomogeneous Broadening $\Gamma_{inh,n}$ Extracted from the Simultaneous Fit of the SFG Spectrum and the FID-SFG[a]

A_n	ω_n (cm^{-1})	Γ_n (cm^{-1})	$T^*_{2,n}$ (fs)	$\Gamma_{inh,n}$ (cm^{-1})
−0.43 ± 0.04	3138.9 ± 11.1	75.1 ± 6.1	70.7 ± 6.8	107.3 ± 17.9
+0.53 ± 0.11	3408.3 ± 11.9	102.1 ± 9.4	51.9 ± 5.9	137.5 ± 15.2

[a]The dephasing time $T^*_{2,n}$ is extracted from Γ_n as $T^*_{2,n} = 1/(2\pi c\Gamma_n)$,[29] and the values of nonresonant susceptibility A_{NR} and phase φ were 0.1 and 0, respectively. Error bars are based on the standard deviation determined from two independent experiments.

but faster than the experimental data, which suggests including a second vibrational oscillator but with an opposite phase to slow down the FID-SFG signal growth. Indeed, after including another oscillator in the simultaneous fit, both frequency and time-domain data were well described by the simulation. Based on these results, shown in Figure 3 and listed in Table 2, it appears that one can indeed separate interfacial water into strongly and weakly hydrogen bonded O−H vibrational populations, with frequencies centered around 3140 cm^{-1} and ∼3410 cm^{-1}, respectively, that are oriented oppositely to each other by having amplitudes with different signs. We note that although these results indicate that there is more than one vibrational oscillator; one cannot exclude the possibility of having more than two peaks in the SFG spectrum. A similar set of data for an independent experiment is shown in Figure S4 and the corresponding fit results in Table S4 of the Supporting Information.

Because the two oscillators are oriented oppositely to each other, the growth of the FID-SFG signal at negative time-delays was slower than the IRF because the two oscillators cancel each other initially. While the low frequency mode has negative amplitude, indicating that its dipole is pointing away from the interface (toward bulk water), the high frequency mode has positive amplitude, implying that it is oriented toward the interface, in agreement with recent phase-sensitive frequency-domain SFG studies.[26]

Based on the homogeneous broadening values extracted from the simultaneous fit, one can estimate the pure dephasing times $T^*_{2,n}$ to be on the order of 51.9 ± 5.9 fs and 70.7 ± 6.9 fs for the weakly and strongly hydrogen bonded O−H vibrational stretches, respectively. These values are about half the total dephasing time previously reported for D_2O/CaF_2, where the FID-SFG decay was on the order of 100−150 fs,[35] but the excitation did not cover both the weakly and strongly hydrogen bonded O−H stretches.[35]

The pure dephasing time values extracted from the simultaneous fit of frequency and time domain SFG measurements are longer than those estimated based on the spectral width of vibrational transitions listed in Table 1. One possible reason for this discrepancy is the contribution of inhomogeneous broadening to the line widths. To test this hypothesis, we performed the simultaneous fit while keeping all the parameters listed in Table 2 fixed, but we excluded the inhomogeneous broadening terms in eqs 2 and 3d. The resulting simulations fits shown in Figure S2 did not describe either the frequency or the time-domain SFG measurements. Next, we performed the simultaneous fit with the inhomogeneous broadening terms in eqs 2 and 3d excluded but we left the other parameters free. The fit plots are shown in Figure S3 and the returned parameters are listed in Table S3. Although the simulation described the frequency-domain SFG spectrum, it did not describe time-domain FID-SFG dynamics. Specifically, at negative time-delays, the rise of the calculated signal was faster than that of the experimental data; in addition, at positive time-delays, the fit missed the decay of the experimental data. Furthermore, the extracted total dephasing times $T_{2,n}$ listed in Table S3 were indeed comparable to those estimated based on frequency domain SFG measurements and faster than the pure dephasing times listed in Table 2.

Surface-specific vSFG was employed in both the frequency and the time domains to study the vibrational dephasing of hydrogen bonded OH stretches in interfacial water. Frequency domain studies revealed two vibrational modes: a low-frequency oscillator representing strongly hydrogen bonded OH stretches that are pointing toward bulk water molecules, and high frequency oscillators representing weakly hydrogen bonded OH stretches that describe the bonds pointed toward the interface. In performing SFG studies in the time-domain, FID-SFG dynamics were captured using an unprecedented temporal resolution of ∼20 fs. The simultaneous fits of frequency and time domain SFG measurements suggested that the strongly and weakly hydrogen bonded OH oscillators centered around 3140 and 3410 cm^{-1} and have pure dephasing times on the order of ∼70 fs and ∼50 fs, respectively.

EXPERIMENTAL SECTION

Sample Preparation. CaF_2 hemicylindrical prisms (13 mm diameter, and 27 mm length) were purchased from Meller Optics. Before the experiment, the prism was cleaned in concentrated sulfuric acid for 3 min and rinsed with deionized water (>18.2 MΩ·cm resistivity) continuously for 5 min. Immediately after rinsing, the prism was dried for 5 min under continuous exposure to compressed nitrogen gas. A similar hemicylinder CaF_2 prism was coated with ∼100 nm thick gold film[36] and used for spectral and temporal characterization of mid-IR and NIR pulses.

Frequency and Time Domain SFG Measurements. The experimental setup for carrying out SFG measurements in the frequency and time domains has been described elsewhere in detail.[20,32] Briefly, a regeneratively amplified Ti:sapphire laser system operating in femtosecond mode[37] produces pulses centered at 800 nm with 150 fs duration at 1 kHz repetition rate that are used to pump two home-built noncollinear optical parametric amplifiers (NOPA1 and NOPA2) to generate ultrabroadband mid-infrared (mid-IR) and near-infrared (NIR) pulses, respectively.[20,32] For frequency domain SFG measurements, the mid-IR pulse is upconverted into an SFG response in the visible (Vis-SFG) using a spectrally narrow portion of the output of the amplifier at 804 nm with fwhm ∼1 nm. For time-domain FID-SFG measurements, the mid-IR pulse is upconverted into an SFG in the NIR (NIR-SFG λ∼ 980 nm) using the temporally compressed NIR signal output of NOPA2 centered at ∼1500 nm.[32] Depending on the experiment, the 1500 nm pulse or the narrowband 804 nm pulse is sent through a motorized stage-delay before it is focused with a 100 mm CaF_2 lens and overlapped with the mid-IR pulse at the CaF_2/H_2O interface at a 55° angle of incidence. The mid-IR angle of incidence on the sample is ∼75°. At the sample, pulse energies were 4 μJ, 2 μJ, and

DOI: 10.1021/acs.jpclett.6b01870
J. Phys. Chem. Lett. 2016, 7, 5080−5085

10 μJ for mid-IR, 1500 nm, and 804 nm pulses, respectively. The reflected Vis-SFG or NIR-SFG (depending on the experiment) beam was collimated then focused into a 200 μm core fiber coupled with a spectrograph-CCD (Andor Shamrock/iDus) detection system. The Vis-SFG and NIR-SFG signals were recorded using a custom built program based on Labview software (National Instruments). Using half-wave plates and polarizers, the Vis-SFG, the 1500 nm, the 804 nm upconverting pulses, and the mid-IR were p-polarized relative to the interface. Time-zero for the FID-SFG measurements is defined as the time-delay where the instrument response function (IRF) intensity, measured at the CaF_2/Au interface, is maximum.

■ ASSOCIATED CONTENT

Supporting Information

The Supporting Information is available free of charge on the ACS Publications website at DOI: 10.1021/acs.jpclett.6b01870.

Results of the simultaneous fit of SFG in frequency and time domains when excluding the inhomogeneous broadening and when considering only one oscillator, and FID-SFG results for an additional independent experiment (PDF)

■ AUTHOR INFORMATION

Corresponding Author

*E-mail: eborguet@temple.edu.

ORCID

Abdelaziz Boulesbaa: 0000-0003-4519-4403

Author Contributions

Both authors have given approval to the final version of the manuscript.

Notes

The authors declare no competing financial interest.

■ ACKNOWLEDGMENTS

The authors acknowledge the National Science Foundation for supporting this work (NSF Grant CHE 1337880).

■ REFERENCES

(1) Jungwirth, P.; Winter, B. Ions at Aqueous Interfaces: FromWater Surface to Hydrated Proteins. *Annu. Rev. Phys. Chem.* **2008**, *59*, 343−366.

(2) Abdi, F. F.; Han, L.; Smets, A. H. M.; Zeman, M.; Dam, B.; van de Krol, R. Efficient solar water splitting by enhanced charge separation in a bismuth vanadate-silicon tandem photoelectrode. *Nat. Commun.* **2013**, *4*, 2195.

(3) Wang, X.; Maeda, K.; Thomas, A.; Takanabe, K.; Xin, G.; Carlsson, J. M.; Domen, K.; Antonietti, M. A metal-free polymeric photocatalyst for hydrogen production from water under visible light. *Nat. Mater.* **2009**, *8*, 76−80.

(4) Hvidt, A. Interactions of Water With Nonpolar Solutes. *Annu. Rev. Biophys. Bioeng.* **1983**, *12*, 1−20.

(5) Kudo, A.; Miseki, Y. Heterogeneous photocatalyst materials for water splitting. *Chem. Soc. Rev.* **2009**, *38*, 253−278.

(6) Moilanen, D. E.; Piletic, I. R.; Fayer, M. D. Water Dynamics in Nafion Fuel Cell Membranes: The Effects of Confinement and Structural Changes on the Hydrogen Bond Network. *J. Phys. Chem. C* **2007**, *111*, 8884−8891.

(7) Oudejans, L.; Miller, R. E. Photofragment Translational Spectroscopy of Weakly Bound Ccomplexes: Probing The Interfragment Correlated Final State Distributions. *Annu. Rev. Phys. Chem.* **2001**, *52*, 607−637.

(8) Asbury, J. B.; Steinel, T.; Fayer, M. D. Hydrogen Bond Networks: Structure and Evolution after Hydrogen Bond Breaking. *J. Phys. Chem. B* **2004**, *108*, 6544−6554.

(9) Stenger, J.; Madsen, D.; Hamm, P.; Nibbering, E. T. J.; Elsaesser, T. Ultrafast Vibrational Dephasing of Liquid Water. *Phys. Rev. Lett.* **2001**, *87*, 027401.

(10) Tokmakoff, A.; Zimdars, D.; Sauter, B.; Francis, R. S.; Kwok, A. S.; Fayer, M. D. Vibrational photon echoes in a liquid and glass: Room temperature to 10 K. *J. Chem. Phys.* **1994**, *101*, 1741−1744.

(11) Nibbering, E. T. J.; Elsaesser, T. Ultrafast Vibrational Dynamics of Hydrogen Bonds in the Condensed Phase. *Chem. Rev.* **2004**, *104*, 1887−1914.

(12) Roychowdhury, S.; Bagchi, B. Vibrational phase relaxation of O−H stretch in bulk water: Role of large amplitude angular jumps and negative cross-correlations among the forces on the O−H bond. *Chem. Phys.* **2008**, *343*, 76−82.

(13) Hogan, P. A.; Fredj, E.; Martens, C. C. Simulation of vibrational dephasing in liquid water using the semiclassical Liouville method. *Chem. Phys. Lett.* **2011**, *510*, 208−211.

(14) Joutsuka, T.; Thompson, W. H.; Laage, D. Vibrational Quantum Decoherence in Liquid Water. *J. Phys. Chem. Lett.* **2016**, *7*, 616−621.

(15) Eaves, J. D.; Tokmakoff, A.; Geissler, P. L. Electric Field Fluctuations Drive Vibrational Dephasing in Water. *J. Phys. Chem. A* **2005**, *109*, 9424−9436.

(16) Richmond, G. L. Structure and Bonding of Molecules at Aqueous Surfaces. *Annu. Rev. Phys. Chem.* **2001**, *52*, 357−389.

(17) Eisenthal, K. B. Liquid Interfaces Probed by Second-Harmonic and Sum-Frequency Spectroscopy. *Chem. Rev.* **1996**, *96*, 1343−1360.

(18) Shen, Y. R.; Ostroverkhov, V. Sum-Frequency Vibrational Spectroscopy on Water Interfaces: Polar Orientation of Water Molecules at Interfaces. *Chem. Rev.* **2006**, *106*, 1140−1154.

(19) Guyot-Sionnest, P. Coherent Processes at Surfaces: Free-Induction Decay and Photon Echo of the Si-H Stretching Vibration for H/Si(111). *Phys. Rev. Lett.* **1991**, *66*, 1489.

(20) Boulesbaa, A.; Borguet, E. Vibrational Dynamics of Interfacial Water by Free Induction Decay Sum Frequency Generation (FID-SFG) at the $Al_2O_3(1120)/H_2O$ Interface. *J. Phys. Chem. Lett.* **2014**, *5*, 528−533.

(21) McGuire, J. A.; Shen, Y. R. Ultrafast Vibrational Dynamics at Water Interfaces. *Science* **2006**, *313*, 1945−1948.

(22) Nihonyanagi, S.; Mondal, J. A.; Yamaguchi, S.; Tahara, T. Structure and Dynamics of Interfacial Water Studied by Heterodyne Detected Vibrational Sum-Frequency Generation. *Annu. Rev. Phys. Chem.* **2013**, *64*, 579−603.

(23) Eftekhari-Bafrooei, A.; Borguet, E. Effect of Surface Charge on the Vibrational Dynamics of Interfacial Water. *J. Am. Chem. Soc.* **2009**, *131*, 12034−12035.

(24) Tuladhar, A.; Dewan, S.; Kubicki, J. D.; Borguet, E. Spectroscopy and Ultrafast Vibrational Dynamics of Strongly Hydrogen Bonded OH Species at the α-$Al_2O_3(11\bar{2}0)/H_2O$ Interface. *J. Phys. Chem. C* **2016**, *120*, 16153−16161.

(25) Hsieh, C. S.; Campen, R. K.; Okuno, M.; Backus, E. H. G.; Nagata, Y.; Bonn, M. Mechanism of vibrational energy dissipation of free OH groups at the air−water interface. *Proc. Natl. Acad. Sci. U. S. A.* **2013**, *110*, 18780−18785.

(26) Khatib, R.; Backus, E. H. G.; Bonn, M.; Perez-Haro, M. J.; Gaigeot, M. R.; Sulpizi, M. Water orientation and hydrogenbond structure at the fluorite/water interface. *Sci. Rep.* **2016**, *6*, 24287.

(27) Scatena, L. F.; Brown, M. G.; Richmond, G. L. Water at Hydrophobic Surfaces: Weak Hydrogen Bonding and Strong Orientation Effects. *Science* **2001**, *292*, 908−912.

(28) Link, S.; El-Sayed, M. A. Optical properties and ultrafast dynamics of metallic nanocrystals. *Annu. Rev. Phys. Chem.* **2003**, *54*, 331−366.

(29) Nihonyanagi, S.; Eftekhari-Bafrooei, A.; Borguet, E. Ultrafast Vibrational Dynamics and Spectroscopy of a Siloxane Self-Assembled Monolayer. *J. Chem. Phys.* **2011**, *134*, 084701−084707.

(30) Roke, S.; Kleyn, A. W.; Bonn, M. Time- vs. Frequency-Domain Femtosecond Surface Sum Frequency Generation. *Chem. Phys. Lett.* **2003**, *370*, 227−232.

DOI: 10.1021/acs.jpclett.6b01870
J. Phys. Chem. Lett. 2016, 7, 5080−5085

(31) Bordenyuk, A. N.; Jayathilake, H.; Benderskii, A. V. Coherent Vibrational Quantum Beats as a Probe of Langmuir−Blodgett Monolayers. *J. Phys. Chem. B* **2005**, *109*, 15941−15949.
(32) Boulesbaa, A.; Isaienko, O.; Tuladhar, A.; Borguet, E. Generation of sub-30-fs microjoule mid-infrared pulses for ultrafast vibrational dynamics at solid/liquid interfaces. *Opt. Lett.* **2013**, *38*, 5008−5011.
(33) Velarde, L.; Wang, H. F. Unified treatment and measurement of the spectral resolution and temporal effects in frequency-resolved sum-frequency generation vibrational spectroscopy (SFG-VS). *Phys. Chem. Chem. Phys.* **2013**, *15*, 19970−19984.
(34) Eftekhari-Bafrooei, A.; Nihonyanagi, S.; Borguet, E. Spectroscopy and Dynamics of the Multiple Free OH Species at an Aqueous/Hydrophobic Interface. *J. Phys. Chem. C* **2012**, *116*, 21734−21741.
(35) Bordenyuk, A. N.; Benderskii, A. V. Spectrally- and time-resolved vibrational surface spectroscopy: Ultrafast hydrogen-bonding dynamics at D_2O/CaF_2 interface. *J. Chem. Phys.* **2005**, *122*, 134713.
(36) Isaienko, O.; Borguet, E. Ultra-Broadband Sum-Frequency Vibrational Spectrometer of Aqueous Interfaces Based on a NonCollinear Optical Parametric Amplifier. *Opt. Express* **2012**, *20*, 547−561.
(37) Bodlaki, D.; Borguet, E. Picosecond infrared optical parametric amplifier for nonlinear interface spectroscopy. *Rev. Sci. Instrum.* **2000**, *71*, 4050−4056.

DOI: 10.1021/acs.jpclett.6b01870
J. Phys. Chem. Lett. 2016, 7, 5080−5085